Editors' Suggestion

First Results on Dark Matter Substructure from Astrometric Weak Lensing

Cristina Mondino,[1,2,*] Anna-Maria Taki,[3,1,†] Ken Van Tilburg,[1,4,‡] and Neal Weiner[1,§]
[1]Center for Cosmology and Particle Physics, Department of Physics, New York University, New York, New York 10003, USA
[2]Perimeter Institute for Theoretical Physics, Waterloo, Ontario N2L 2Y5, Canada
[3]Institute for Fundamental Science, University of Oregon, Eugene, Oregon 97403, USA
[4]Center for Computational Astrophysics, Flatiron Institute, New York, New York 10010, USA

(Received 5 March 2020; accepted 10 August 2020; published 9 September 2020)

Low-mass structures of dark matter (DM) are expected to be entirely devoid of light-emitting regions and baryons. Precisely because of this lack of baryonic feedback, small-scale substructures of the Milky Way are a relatively pristine testing ground for discovering aspects of DM microphysics and primordial fluctuations on subgalactic scales. In this Letter, we report results from the first search for Galactic DM subhalos with time-domain astrometric weak gravitational lensing. The analysis is based on a matched-filter template of local lensing corrections to the proper motion of stars in the Magellanic Clouds. We describe a data analysis pipeline detailing sample selection, background subtraction, and the handling of outliers and other systematics. For tentative candidate lenses, we identify a signature based on an anomalous parallax template that can unequivocally confirm the presence of a DM lens, opening up prospects for robust discovery potential with full time-series data. We present our constraints on substructure fraction $f_l \lesssim 5$ at 90% C.L. (and $f_l \lesssim 2$ at 50% C.L.) for compact lenses with radii $r_l < 1$ pc, with best sensitivity reached for lens masses M_l around 10^7–$10^8\ M_\odot$. Parametric improvements are expected with future astrometric datasets; by end of mission, *Gaia* could reach $f_l \lesssim 10^{-3}$ for these massive point-like objects and be sensitive to lighter and/or more extended subhalos for $\mathcal{O}(1)$ substructure fractions.

DOI: 10.1103/PhysRevLett.125.111101

Introduction.—The precise nature of the constituents of the dark matter (DM) and their microphysical properties is not known. Nevertheless, a wealth of information has been collected about DM's macroscopic properties and behavior from its minimal coupling to gravity and its resulting gravitational influence. In the linear theory of structure formation, a fluid with adiabatic fluctuations and vanishing sound speed clusters in a way that shows remarkable agreement with observations of the cosmic microwave background [1,2], the Lyman-α forest [3–5], and large-scale structures [6–8]. This evolution has been probed over comoving length scales between 0.1 and 10^4 Mpc starting from a time when the Universe and the DM were more than 10 orders of magnitude denser than at the present time. N-body simulations [9–15] extend these predictions to smaller physical length scales and into the nonlinear regime, matching observations of galactic rotation curves [16–20], statistical dispersion relations [21–26], weak [27–31] and strong [32–34] gravitational lensing, and the distribution and abundance of satellite galaxies [35–37]. These complementary bodies of evidence not only put the existence of DM on a strong footing, they also provide knowledge about its coarse-grained phase-space distribution, indispensable input to searches for any nonminimal DM couplings.

Detection of smaller DM structures becomes increasingly challenging due to their lower light-to-mass ratios; DM halos with scale masses below $10^8\ M_\odot$ do not harbor conditions for star formation and are thus entirely dark [38–40]. Methods reliant on the minimal coupling to gravity include fluctuations in extragalactic strong gravitational lenses [41–61], stellar wakes in the Milky Way (MW) disk [62] and halo [63], diffraction of gravitational waves [64], photometric irregularities of microcaustic light curves [65], and perturbations of cold stellar streams [66–72] (with tentative positive detections [73,74]). These techniques show significant promise but are indirect or applicable to extragalactic structures only. Direct searches for MW substructure have so far been confined to transients in photometric lensing [75–80] and pulsar timing [81–87], which only produce detectable signals for ultracompact objects such as black holes but not for more extended structures such as DM halos that collapse after matter-radiation equality.

In this Letter, we present the first results of a qualitatively new class of searches for Galactic DM substructure using time-domain astrometric weak gravitational lensing. Reference. [88] proposed several categories of observables to this effect and forecasted their sensitivity on upcoming astrometric surveys. We employ a refined version of their "local velocity template" on a sample of Small and Large Magellanic Cloud (SMC and LMC, respectively) stars in *Gaia*'s second data release (DR2). Our data analysis

constitutes a robust, optimal, matched-filter-based search for local distortions of the proper motion field of background sources produced by the gravitational lensing of intervening foreground compact DM subhalos. We find no evidence of this effect. Given a population of subhalos with fixed mass M_l, characteristic radius r_l, and number density $f_l\rho_{\rm DM}/M_l$, we set a constraint on $f_l \lesssim 5$ at 90% C.L. (and $f_l \lesssim 2$ at 50% C.L.) for $M_l \sim 10^8\ M_\odot$ and $r_l \lesssim 1$ pc. Currently limited by statistical instrumental uncertainties, we expect the reach to the combination $f_l M_l^2/r_l^3$ to improve as $\propto t_{\rm int}^{-9/2}$, with the integration time $t_{\rm int}$ set to increase fivefold by *Gaia*'s end of mission.

A localized discovery of dark low-mass substructures with our technique, possible with future astrometric surveys, would be a watershed event. Because of the absence of baryonic feedback, their abundance, mass function, and density profiles would provide a transparent window on the primordial fluctuation spectrum and the DM's transfer function on comoving scales below 0.1 Mpc. It would probe the spectrum of adiabatic perturbations produced from the inflationary stage after the one measured in the cosmic microwave background [89,90] and the Ly-α forest [91]. Their discovery (nonobservation) would rule out (provide evidence for) small-scale structure suppression, unavoidable predictions of light fermion ("warm") [92–94] and ultralight scalar ("fuzzy") [95–97] DM models. The enhanced-density subhalos searched in this work can arise in motivated scenarios that include increased primordial curvature fluctuations (that can generate primordial black holes [98,99], ultracompact minihalos [100,101], and supermassive DM clumps [102]); small-scale isocurvature fluctuations produced from, e.g., a phase transition in the DM sector [103–105]; early-Universe structure growth in axion DM models with large misalignment [106]; and late-Universe dissipation and self-interactions of DM [107–109].

Lensing signal.—The physical effect under consideration is time-domain weak gravitational lensing of the astrometric kind, summarized in Fig. 1. "Weak" refers to the regime where the impact parameter is much larger than the Einstein radius of the lens and one image of the source is resolved by the observer, and "astrometric" refers to the effect of angular deflection of the source's light centroid. True celestial positions $\boldsymbol{\theta}_i$ are unknown *a priori*, rendering the angular deflection $\Delta\boldsymbol{\theta}_{il}$ of source i by lens l unobservable in practice.

Ref. [88] proposed leveraging *time-domain* lensing effects due to the relative rate of change in impact parameter $\dot{\mathbf{b}}_{il} \simeq \mathbf{v}_l$ in the reference frame of the observer. (We ignore the small contribution of the distant background source motions to $\dot{\mathbf{b}}_{il}$.) The leading observable in the time domain (i.e., to first order in $\mathbf{v}_l$) is a lensing correction to the proper motion $\boldsymbol{\mu}_i$:

$$\Delta\boldsymbol{\mu}_{il} \equiv \Delta\dot{\boldsymbol{\theta}}_{il} = \frac{D_{li}}{D_i}\frac{4G_N M_l v_l}{r_l^2}\tilde{\boldsymbol{\mu}}_i(\beta_l, \boldsymbol{\beta}_{il}, \hat{\mathbf{v}}_l), \tag{1}$$

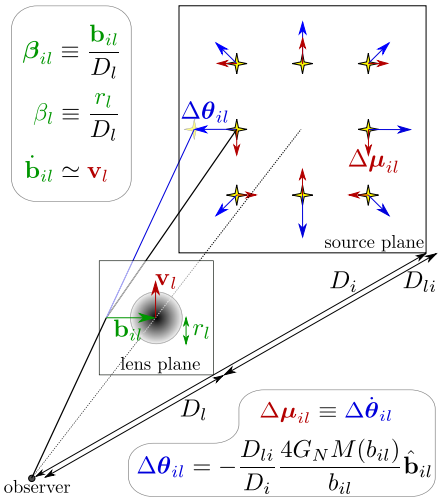

FIG. 1. Diagram of gravitational lensing geometry of sources i by a lens l. The impact parameter is $\mathbf{b}_{il}$, its rate of change $\mathbf{v}_l$, the lens radius r_l, and respective line-of-sight distances D_i and D_l. In celestial coordinates, the angular impact parameter is $\boldsymbol{\beta}_{il} \equiv \boldsymbol{\theta}_i - \boldsymbol{\theta}_l$, angular lens radius β_l. The angular displacement $\Delta\boldsymbol{\theta}_{il}$ (blue, monopole pattern) is not constant in time, leading to lensing corrections $\Delta\boldsymbol{\mu}_{il}$ to the sources' proper motions $\boldsymbol{\mu}_i$ (red, dipole pattern).

where G_N is Newton's gravitational constant, r_l a characteristic lens radius, and $M_l = 4\pi\int_0^\infty {\rm d}r r^2\rho_l(r)$ the mass of the lens with 3D density profile $\rho_l(r)$. We will always assume $D_{li} \sim D_i$. The unitless 2D spatial profile of the distortion is

$$\tilde{\boldsymbol{\mu}}_i(\beta_l, \boldsymbol{\beta}_{il}, \hat{\mathbf{v}}_l) = \frac{\tilde{M}_l(\beta_{il})}{\beta_{il}^2/\beta_l^2}[2\hat{\boldsymbol{\beta}}_{il}(\hat{\boldsymbol{\beta}}_{il}\cdot\hat{\mathbf{v}}_l) - \hat{\mathbf{v}}_l] - \frac{\partial_{\beta_{il}}\tilde{M}(\beta_{il})}{\beta_{il}/\beta_l^2}\hat{\boldsymbol{\beta}}_{il}(\hat{\boldsymbol{\beta}}_{il}\cdot\hat{\mathbf{v}}_l) \tag{2}$$

with $M(b) = 2\pi\int_{-\infty}^{\infty}{\rm d}z\int_0^b {\rm d}b' b'\rho_l(\sqrt{z^2+b'^2})$ the enclosed lens mass within a cylinder oriented along the line of sight (z direction) with radius equal to b, cfr. Fig. 1, and $\tilde{M}(\beta_{il}) \equiv M(b_{il})/M_l$. We also introduced the lens angular size $\beta_l \equiv r_l/D_l$ and angular impact parameter $\boldsymbol{\beta}_{il} \equiv \mathbf{b}_{il}/D_l$.

The primary lensing signature is thus a distortion in the angular velocity of background sources with a magnitude given by the prefactor in Eq. (1) and the characteristic spatial pattern of Eq. (2), which is a *universal* dipole pattern for sources far outside the lens radius β_{il}/β_l and depends on the lens density profile for sources eclipsed by the lens. For specificity, we assume the lens density profile

$$\rho_l(r) = \frac{M_l}{4\pi}\frac{\exp\{-\frac{r^2}{2r_l^2}\}}{r r_l^2} \tag{3}$$

throughout the main text. The above profile exhibits the $1/r$ cusp of the Navarro-Frenk-White (NFW) profile but maximizes the signal since it has no significant mass outside the

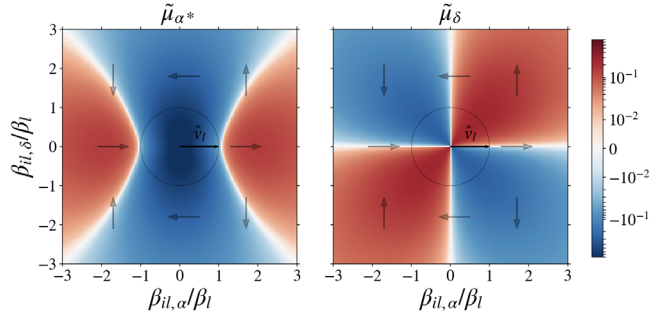

FIG. 2. Right ascension (α, left) and declination (δ, right) components of the angular velocity vector profile $\tilde{\boldsymbol{\mu}}_i$ of Eq. (2) as a function of angular separation $\boldsymbol{\beta}_{il}$ for the lens density profile of Eq. (3). The lens has angular size β_l and is moving in the direction $\hat{\mathbf{v}}_l = \hat{\mathbf{v}}_\alpha$.

scale radius r_l [the radius where $\partial_{\ln r}(\ln \rho_l) = -2$], which would contribute to the lens mass abundance but only minimally to the lensing signal. The analysis presented here can easily be adapted to other density profiles, such as a pure Gaussian or a tidally truncated NFW profile, by properly choosing the function $\tilde{M}_l$ in Eq. (2). In the Supplemental Material [110], we investigate a profile-agnostic approach by truncating the lensing signal at r_l. In Fig. 2, we display the angular velocity distortion pattern of Eq. (2) resulting from the density profile in Eq. (3).

We take the lenses' spatial distribution across the Milky Way to follow that of the Galactic DM halo with a fiducial NFW profile

$$\rho(\mathbf{r}) = \frac{4\rho_s}{\frac{r}{R_s}[1+\frac{r}{R_s}]^2}, \qquad R_s = 18 \text{ kpc}, \qquad \rho_s = 0.003 \frac{\mathrm{M}_\odot}{\mathrm{pc}^3}, \tag{4}$$

with r the galactocentric radius, and the observer located at $r_\odot = 8$ kpc [111]. We assume a transverse lens velocity distribution for the subhalos given by

$$p_v(\mathbf{v}_l) = \frac{1}{2\pi\sigma_v^2}\exp\left[-\frac{(\mathbf{v}_l - \mathbf{v}_0)^2}{2\sigma_v^2}\right], \qquad \sigma_v \simeq 166\frac{\mathrm{km}}{\mathrm{s}}, \tag{5}$$

where $\mathbf{v}_0$ denotes a 2D velocity vector equal in magnitude and opposite to the observer's velocity projected on the plane perpendicular to the line of sight. We take the observer's velocity to be the Solar System's velocity of 238 km/s in the Galactic equatorial plane ($b \approx 0$, $l \approx 270°$). In the following, we will ignore the additional annual rotation around the Sun but will return to this parallax effect in the Discussion.

Template method.—We utilize a *local* test statistic $\mathcal{T}$ that computes the overlap of the velocity field of background sources with the one induced by a tentative lens candidate with angular position $\boldsymbol{\theta}_t$, angular scale β_t, and effective lens velocity direction $\hat{\mathbf{v}}_t$ [88]:

$$\mathcal{T}(\boldsymbol{\theta}_t, \beta_t, \hat{\mathbf{v}}_t) \equiv \sum_i \frac{\boldsymbol{\mu}_i \cdot \tilde{\boldsymbol{\mu}}_i(\beta_t, \boldsymbol{\beta}_{it}, \hat{\mathbf{v}}_t)}{\sigma_{\mu,i}^2}, \tag{6}$$

where $\boldsymbol{\mu}_i \equiv \{\mu_{i,\alpha*}, \mu_{i,\delta}\} = \{\mu_{i,\alpha}\cos\delta_i, \mu_{i,\delta}\}$ is the proper motion vector of the ith star, and $\sigma_{\mu,i}^2 \equiv \sigma_{\mu_\alpha,i}^2 + \sigma_{\mu_\delta,i}^2$ is the measured variance over the chosen stellar population. The velocity template vector $\tilde{\boldsymbol{\mu}}_i$ is a matched filter to the lens-induced velocity vector profile and is given in Eq. (2) generally and for the specific density profile of Eq. (3) in Fig. 2. $\mathcal{T}$ depends on the lens position through the angular impact parameters $\boldsymbol{\beta}_{it} \equiv \boldsymbol{\theta}_t - \boldsymbol{\theta}_i$.

We define the normalization factor

$$\mathcal{N}^2(\boldsymbol{\theta}_t, \beta_t) \equiv \sum_i \frac{|\tilde{\boldsymbol{\mu}}_i(\beta_t, \boldsymbol{\beta}_{it}, \hat{\mathbf{v}}_t)|^2}{\sigma_{\mu,i}^2}, \tag{7}$$

that acts as a figure of merit for the sensitivity of a candidate lens position and radius: large values indicate the presence of numerous low-noise stars within β_t around the template. In the absence of a lensing signal, one expects vanishing mean $\langle\mathcal{T}\rangle_{\text{noise}}$ with a variance $\langle\mathcal{T}^2\rangle_{\text{noise}} = \mathcal{N}^2 \sim \Sigma\beta_t^2/\sigma_\mu^2$ with Σ the typical local angular number density of background sources.

In the presence of a lens and with template parameters perfectly matched to those of the lens (i.e., $\boldsymbol{\theta}_t = \boldsymbol{\theta}_l, \beta_t = \beta_l$, and $\hat{\mathbf{v}}_t = \hat{\mathbf{v}}_l$), the test statistic is expected to evaluate to $\langle\mathcal{T}\rangle_{\text{signal}} \simeq \mathcal{N}^2 4G_N M_l v_l/r_l^2$ for a nearby lens $D_l \ll D_i$. The *local* signal-to-noise ratio $\text{SNR} = \langle\mathcal{T}\rangle_{\text{signal}}/\sqrt{\langle\mathcal{T}^2\rangle_{\text{noise}}}$ is then

$$\text{SNR} = \frac{\langle\mathcal{T}\rangle_{\text{signal}}}{\mathcal{N}} \simeq \frac{4G_N M_l v_l}{r_l^2}\mathcal{N} \sim \frac{4G_N M_l v_l\sqrt{\Sigma}}{r_l D_l \sigma_\mu}, \tag{8}$$

and is generally largest for the most nearby, massive, compact, and fast-moving lenses in front of high-density, low-noise regions.

The true lens properties are unknown *a priori*. $\mathcal{T}$ is evaluated over a dense grid in $\boldsymbol{\theta}_t$ and β_t, introducing the basis $\{\hat{\boldsymbol{\alpha}}, \hat{\boldsymbol{\delta}}\}$ for the template direction $\hat{\mathbf{v}}_t$. We define a *global* test statistic $\mathcal{R}$ for detecting the proper motion distortion of a *single* lens across a certain patch of sky. After marginalizing over the lens velocity prior from Eq. (5), we obtain (see Supplemental Material [110] for derivation)

$$\mathcal{R} = \sup_{\boldsymbol{\theta}_t, \beta_t}\left[\ln\frac{\rho}{\beta_t^4} + \frac{C^2\sigma_v^2\mathcal{N}^2(\frac{|\boldsymbol{\mathcal{T}}|^2}{\mathcal{N}^2} - \frac{v_0^2}{\sigma_v^2}) + 2C\boldsymbol{\mathcal{T}}\cdot\mathbf{v}_0}{2(1+C^2\sigma_v^2\mathcal{N}^2)}\right] \tag{9}$$

with $\rho = \rho(\boldsymbol{\theta}_t, r_l/\beta_t)$ from Eq. (4), $C = 4G_N M_l/r_l^2$, and $\boldsymbol{\mathcal{T}} \equiv \{\mathcal{T}(\boldsymbol{\theta}_t, \beta_t, \hat{\boldsymbol{\alpha}}), \mathcal{T}(\boldsymbol{\theta}_t, \beta_t, \hat{\boldsymbol{\delta}})\}$. Roughly speaking, it corresponds to taking the largest value of $\boldsymbol{\mathcal{T}}/\mathcal{N}$ across the densely scanned grid of $\{\boldsymbol{\theta}_t, \beta_t\}$, but it also properly accounts for variations in $\mathcal{N}(\theta_t, \beta_t)$, priors on the 3D location of the lens, and the $\mathbf{v}_l$ asymmetry in Eq. (5) ($\langle\boldsymbol{\mathcal{T}}\rangle_{\text{signal}} \propto \mathbf{v}_0$).

Data processing.—Data sample: For our analysis, we choose astrometric data on the LMC and SMC from *Gaia*'s second data release [112,113]. They have large stellar angular number densities and low proper motion dispersion (intrinsic and instrumental), maximizing the SNR of Eq. (8) with a high $\sqrt{\Sigma}/\sigma_\mu$. Their large combined angular area also increases the probability of at least one nearby (low D_l) lens.

To avoid foreground contamination, we select sources without evidence of parallax ($\varpi/\sigma_\varpi < 2$) in a square of 10° sidelength centered on $(\alpha, \delta) = (78.77°, -69.01°)$ for the LMC and 8° on $(12.80°, -73.15°)$ for the SMC. For the SMC, we impose $|\mu_{\alpha*} - 0.685\ \mathrm{mas/y}| < 2\ \mathrm{mas/y}$ and $|\mu_\delta + 1.230\ \mathrm{mas/y}| < 2\ \mathrm{mas/y}$ to cut out the foreground NGC 104 and 362 globular clusters [114]. Poor astrometric solutions were avoided with a cut on renormalized unit weight error of RUWE < 1.4 [115]. We summarize our data processing operations here; more details can be found in the Supplemental Material [110], which includes Ref. [116].

Removal of dense clusters: Overdense stellar clusters generally move coherently and independently from the bulk stars in the Magellanic Clouds (MCs) and are thus contaminants from our perspective. We calculate a smoothed angular number density map $\Sigma_{\rm sm}(\boldsymbol{\theta})$ with a Gaussian kernel of angular radius 0.1° and a pixelated angular number density map $\Sigma(\boldsymbol{\theta})$ with pixels of size 0.1°/3. Density outliers are removed by excising regions for which $\Sigma > 3\Sigma_{\rm sm}$.

Motion subtraction and outlier removal: We subtract the large-scale proper motion and remove stars that are not bound to the MCs. Operationally, we define a motion field $\boldsymbol{\mu}(\boldsymbol{\theta}_p) = \sum_{i\in p} \boldsymbol{\mu}_i \sigma_{\mu,i}^{-2} / \sum_{i\in p} \sigma_{\mu,i}^{-2}$ in square pixels p of 0.05°, from which we calculate a smoothed motion field $\boldsymbol{\mu}_{\rm sm}(\boldsymbol{\theta})$ with Gaussian kernel of radius 0.1°. We then construct a list of stellar motions with large-scale motion subtracted: $\boldsymbol{\mu}_{{\rm sub},i} \equiv \boldsymbol{\mu}_i - \boldsymbol{\mu}_{\rm sm}(\boldsymbol{\theta}_i)$. Stars with $\mu_{{\rm sub},i} > 3\sigma_{\mu,i} + \mu_{\rm esc}$ are removed, where $\mu_{\rm esc}$ is the (proper) escape velocity. The outlier removal slightly biases $\boldsymbol{\mu}_{\rm sm}$, so the process is iterated another two times with the remaining stars.

Effective error: After the above procedures, we arrive at a proper motion field with $\langle \boldsymbol{\mu}_{{\rm sub},i} \rangle \simeq 0$ but where the observed variance $\sigma^2_{\mu,\rm eff} \equiv \langle \mu^2_{{\rm sub},i} \rangle$ still exceeds the *Gaia*-reported variance $\sigma^2_{\mu,\rm Gaia} \equiv \langle \sigma^2_{\mu,i} \rangle$. This discrepancy is due to intrinsic (proper) velocity dispersion $\sigma_{\mu,\rm intrinsic}$ in the MCs as well as unmodeled instrumental systematics, unresolved binaries and double stars, and other astrometric misfits [117,118]. In Fig. 3, we plot the number of stars (red), $\sigma_{\mu,\rm eff}$ (blue), $\sigma_{\mu,\rm Gaia}$ (green), and $\sigma_{\mu,\rm intrinsic}$ (gray) [119,120] in bins of 0.1 width in G magnitude for the LMC (thick) and SMC (thin). In the following analysis, we use the G-mag-dependent $\sigma^2_{\mu,\rm eff}$ as the inverse weight factor in Eqs. (6) and (7).

Analysis and results.—Evaluation of test statistics: We compute $\boldsymbol{\mathcal{T}}(\boldsymbol{\theta}_t, \beta_t)$ and $\mathcal{N}(\boldsymbol{\theta}_t, \beta_t)$ over a coarse square grid

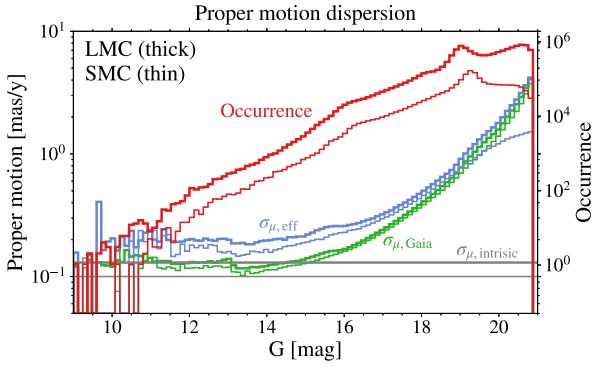

FIG. 3. Number of stars (red), observed ($\sigma_{\mu,\rm eff}$, blue), reported ($\sigma_{\mu,Gaia}$, green), and intrinsic ($\sigma_{\mu,\rm intrinsic}$, gray) proper motion dispersion as a function of stellar G magnitude for the LMC (thick) and SMC (thin).

with lattice constant $\beta_{\rm scan} = 0.9 \times \beta_t$ for a fixed list of 58 β_t values evenly spaced between 0.0015° and 0.03°. The results of this procedure for four angular scales are displayed for the LMC data in Fig. 4: $\boldsymbol{\mathcal{T}}/\mathcal{N}$ (of which only the norm is displayed) follows a 2D normal distribution out to 5 sigma, as expected from background. At each β_t, we then identify coarse lattice sites at which $\mathcal{T} > 0.25\max_{\boldsymbol{\theta}_t}\mathcal{T}$ and compute $\boldsymbol{\mathcal{T}}, \mathcal{N}$ over sets of finer grids with lattice constant $\beta'_{\rm scan} = \beta_{\rm scan}/3$ around these high-$\mathcal{T}$ sites. This finer scanning procedure is iterated once more with $\beta''_{\rm scan} = \beta'_{\rm scan}/3$ at lattice sites at which $\mathcal{T} > 0.5\max_{\boldsymbol{\theta}_t}\mathcal{T}$. For each parameter space point in the 3D space $\{M_l, r_l, f_l\}$, we calculate $\mathcal{R}$ as defined in Eq. (9) from the finest grid of $\boldsymbol{\mathcal{T}}, \mathcal{N}$ values over the combined LMC & SMC sample.

Signal injection: For each point in $\{M_l, r_l, f_l\}$, we create a minimum of 100 simulations of lensing signal [in accordance with Eqs. (3), (4), and (5)] and data-driven stochastic noise (see Supplemental Material [110]). The simulations are run through the same analysis pipeline (in particular also the motion subtraction and outlier removal)

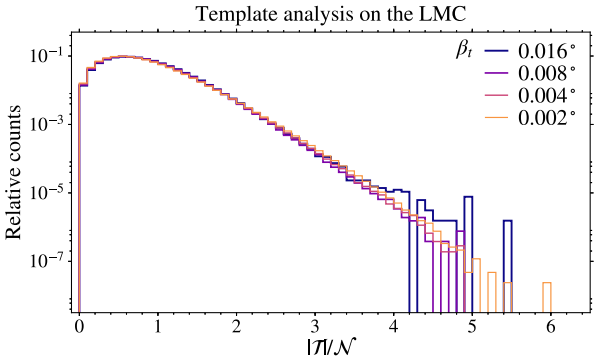

FIG. 4. Histograms of the local test statistic $|\boldsymbol{\mathcal{T}}(\boldsymbol{\theta}_t, \beta_t)|/\mathcal{N}(\boldsymbol{\theta}_t, \beta_t)$, where $\boldsymbol{\mathcal{T}} \equiv \{\mathcal{T}(\boldsymbol{\theta}_t, \beta_t, \hat{\boldsymbol{\alpha}}), \mathcal{T}(\boldsymbol{\theta}_t, \beta_t, \hat{\boldsymbol{\delta}})\}$, evaluated at all template locations $\boldsymbol{\theta}_t$ and different angular template radii β_t for the coarse-grid analysis on the LMC data sample.

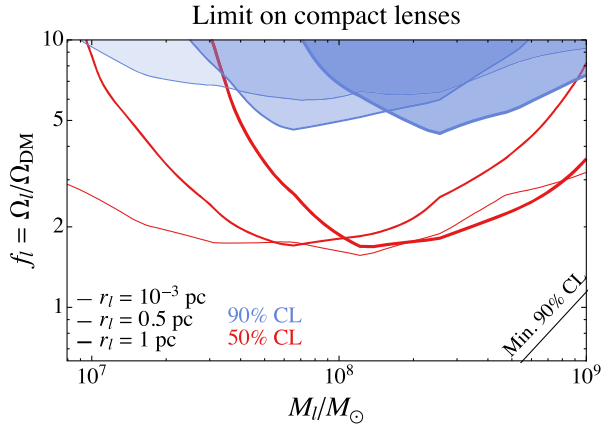

FIG. 5. Constraints from the MCs' velocity template analysis on the fractional dark matter abundance f_l of compact objects with mass M_l and density profile given in Eq. (3), for different compact object radii $r_l = 10^{-3}$, 0.5, and 1 pc. The constraint for the smallest radius is equivalent to the one for point-like objects ($r_l = 2G_N M_l$) given the angular number density of stars. Above the diagonal line at the bottom right, at least one subhalo eclipses the data sample with 90% probability.

as the actual data, yielding a distribution of $\mathcal{R}$ values for each parameter space point in $\{M_l, r_l, f_l\}$. If 90% (50%) of the simulations have an $\mathcal{R}$ value larger than the observed $\mathcal{R}$ value for any parameter space point, then that point is excluded at 90% (50%) C.L. As a cross-check on our limit-setting strategy, we also generated 60 noise-only simulations and found that the mean $\mathcal{R}$ value across a handful of parameter space points is 92%–97% that of the observed value. This observation implies that no significant excess is present in the data and that our noise injection is conservative.

Constraints: The resulting limits are displayed in the (M_l, f_l) plane in Fig. 5 for three values of r_l. The current dataset is sensitive to substructure fractions f_l between 1 and 5 for M_l between $10^6\ M_\odot$ and $10^9\ M_\odot$, while the 90% C.L. limit reaches $f_l \approx 5$ only at the most sensitive parameter-space points. Assuming that all the subhalos have the same mass M_l does not significantly affect the constraints; the limit on f_l at any (M_l, r_l) can be approximately interpreted as a limit on the integrated subhalos over, e.g., a double logarithmic bin around that parameter-space point [88]. The comparatively worse limit for $r_l = 0.5$ pc (relative to $r_l = 10^{-3}$ pc, 1 pc) at high M_l is driven by a relatively high maximum $\mathcal{T}/\mathcal{N}$ value for $\beta_t = 0.002°$ near $\boldsymbol{\theta}_t \approx (82.54°, -69.76°)$, consistent with a statistical fluctuation for a background-only hypothesis. Our analysis does not yet rule out a subcomponent of DM in the form of compact objects but excludes a relative overdensity of subhalos in the region of the sky that eclipses the MCs. Note that such an overdensity has been predicted in simulations of MW-like halos that include LMC analogs [121] and confirmed by the observation of LMC-associated satellites in *Gaia* [122] and the Dark Energy Survey [121]. The subhalos in this parameter space are safeguarded against tidal stripping due to their high density [123]; at the high-mass end, nearby subhalos are subject to dynamical friction that could significantly alter their evolution in the Galaxy [124].

Discussion.—We presented results and limits from the first analysis leveraging precision astrometry data and time-domain weak gravitational lensing to look for Galactic substructure. A simple modification of our analysis technique can also unambiguously *confirm* tentative local lensing signals. The rate of change of the impact parameter receives periodic contributions from the Earth's motion around the Sun with known phase, direction, and magnitude of ∼30 km/s. This lensing-induced "anomalous parallax" motion is guaranteed to be present if a tentative signal of correlated linear stellar motions is due to astrometric weak lensing. The out-of-phase contribution to the parallax motion cannot be captured by the current astrometric solution delivered by the *Gaia* collaboration. A proper analysis on the full time-series data is required to detect the combined linear and circular lensing-induced motions. The parallax effect is almost an order of magnitude smaller, and its error has less favorable scaling with integration time than the linear motion ($\sigma_{\mu,\varpi}/\sigma_\mu \sim t_{\rm int}/1$ yr). However, this signature will always be statistics-limited insofar that it cannot be faked by intrinsic stellar motions. This latter observation opens up the possibility of astrometric lensing searches for dark matter on *Gaia*'s *entire* dataset, including more precisely measured nearby stars rather than the distant MCs.

Our constraints are statistics-limited now and for the foreseeable future, as the figure of merit $\sqrt{\Sigma}/\sigma_{\mu,\rm eff}$ is largest for relatively faint stars with G > 16 and the vast majority of MC stars have G > 19. With integration time $t_{\rm int}$, currently at 22 months for *Gaia* DR2, we expect the proper motion error to scale at least as fast as $\sigma_{\mu,\rm eff} \propto t_{\rm int}^{-3/2}$. The scaling will likely be faster as more stars are added, binaries and double stars are resolved, and modeling of telescope systematics improves with time. Note that Eq. (8) is valid for $r_l \gtrsim 1$ pc in this context and that the closest lens at $\langle \min_l D_l \rangle \propto (M_l/f_l)^{1/3}$ drives the sensitivity. We project that the sensitivity to the combination $f_l M_l^2/r_l^3$ will scale as $\sigma^3_{\mu,\rm eff} \propto t_{\rm int}^{-9/2}$ or better, leading to a limit on substructure fraction f_l improved by 3 orders of magnitude with *Gaia's* final data release and yielding promising prospects for other astrometric surveys.

We thank Asimina Arvanitaki, Masha Baryakhtar, David Hogg, Junwu Huang, Mariangela Lisanti, Siddharth Mishra-Sharma, and Oren Slone for helpful discussions. K. V. T.'s research is funded by the Gordon and Betty Moore Foundation through Grant No. GBMF7392. C. M. is supported by the Thomas J. Moore dissertation fellowship. A. M. T. is supported in part by the U.S. Department of Energy under Grant No. DE-SC0011640. N. W. is funded by the Simons Foundation and by the NSF under Grants

No. PHY-1620727 and PHY-1915409. This project was developed in part at the April 2018 NYC Gaia DR2 Workshop and the 2018 NYC Gaia Sprint at the Center for Computational Astrophysics of the Flatiron Institute. This work has made use of data from the European Space Agency (ESA) mission *Gaia* (https://www.cosmos.esa.int/gaia), processed by the *Gaia* Data Processing and Analysis Consortium (DPAC, https://www.cosmos.esa.int/web/gaia/dpac/consortium). Funding for the DPAC has been provided by national institutions, in particular the institutions participating in the *Gaia* Multilateral Agreement.

*Corresponding author.
cm4001@nyu.edu
†Corresponding author.
ataki@uoregon.edu
‡Corresponding author.
kenvt@nyu.edu
§Corresponding author.
neal.weiner@nyu.edu

[1] P. A. Ade, N. Aghanim, M. Arnaud, M. Ashdown, J. Aumont, C. Baccigalupi, A. Banday, R. Barreiro, J. Bartlett, N. Bartolo *et al.*, Astron. Astrophys. **594**, A13 (2016).
[2] N. Aghanim, Y. Akrami, M. Ashdown, J. Aumont, C. Baccigalupi, M. Ballardini, A. Banday, R. Barreiro, N. Bartolo, S. Basak *et al.*, arXiv:1807.06209.
[3] U. Seljak, A. Slosar, and P. McDonald, J. Cosmol. Astropart. Phys. 10 (2006) 014.
[4] M. Blomqvist, H. d. M. d. Bourboux, N. G. Busca, V. d. S. Agathe, J. Rich, C. Balland, J. E. Bautista, K. Dawson, A. Font-Ribera, J. Guy *et al.*, Astron. Astrophys. **629**, A86 (2019).
[5] V. d. S. Agathe, C. Balland, H. d. M. d. Bourboux, N. G. Busca, M. Blomqvist, J. Guy, J. Rich, A. Font-Ribera, M. M. Pieri, J. E. Bautista *et al.*, Astron. Astrophys. **629**, A85 (2019).
[6] W. J. Percival and M. White, Mon. Not. R. Astron. Soc. **393**, 297 (2009).
[7] C. Howlett, A. J. Ross, L. Samushia, W. J. Percival, and M. Manera, Mon. Not. R. Astron. Soc. **449**, 848 (2015).
[8] P. Zarrouk, E. Burtin, H. Gil-Marín, A. J. Ross, R. Tojeiro, I. Pâris, K. S. Dawson, A. D. Myers, W. J. Percival, C.-H. Chuang *et al.*, Mon. Not. R. Astron. Soc. **477**, 1639 (2018).
[9] V. Springel, J. Wang, M. Vogelsberger, A. Ludlow, A. Jenkins, A. Helmi, J. F. Navarro, C. S. Frenk, and S. D. White, Mon. Not. R. Astron. Soc. **391**, 1685 (2008).
[10] J. Diemand, M. Kuhlen, P. Madau, M. Zemp, B. Moore, D. Potter, and J. Stadel, Nature (London) **454**, 735 (2008).
[11] M. Boylan-Kolchin, V. Springel, S. D. White, A. Jenkins, and G. Lemson, Mon. Not. R. Astron. Soc. **398**, 1150 (2009).
[12] J. Stadel, D. Potter, B. Moore, J. Diemand, P. Madau, M. Zemp, M. Kuhlen, and V. Quilis, Mon. Not. R. Astron. Soc. Lett. **398**, L21 (2009).
[13] S. Garrison-Kimmel, M. Boylan-Kolchin, J. S. Bullock, and K. Lee, Mon. Not. R. Astron. Soc. **438**, 2578 (2014).
[14] M. Vogelsberger, S. Genel, V. Springel, P. Torrey, D. Sijacki, D. Xu, G. Snyder, D. Nelson, and L. Hernquist, Mon. Not. R. Astron. Soc. **444**, 1518 (2014).
[15] W. A. Hellwing, C. S. Frenk, M. Cautun, S. Bose, J. Helly, A. Jenkins, T. Sawala, and M. Cytowski, Mon. Not. R. Astron. Soc. **457**, 3492 (2016).
[16] V. C. Rubin and W. K. Ford, Jr., Astrophys. J. **159**, 379 (1970).
[17] K. C. Freeman, Astrophys. J. **160**, 811 (1970).
[18] D. Rogstad and G. Shostak, Astrophys. J. **176**, 315 (1972).
[19] R. N. Whitehurst and M. S. Roberts, Astrophys. J. **175**, 347 (1972).
[20] M. Roberts and A. Rots, Astron. Astrophys. **26**, 483 (1973).
[21] F. Zwicky, Helv. Phys. Acta **6**, 110 (1933).
[22] S. Smith, Astrophys. J. **83**, 23 (1936).
[23] F. Zwicky, Astrophys. J. **86**, 217 (1937).
[24] M. Girardi, G. Giuricin, F. Mardirossian, M. Mezzetti, and W. Boschin, Astrophys. J. **505**, 74 (1998).
[25] K. Rines and A. Diaferio, Astron. J. **132**, 1275 (2006).
[26] M. R. Becker, T. McKay, B. Koester, R. Wechsler, E. Rozo, A. Evrard, D. Johnston, E. Sheldon, J. Annis, E. Lau *et al.*, Astrophys. J. **669**, 905 (2007).
[27] N. Kaiser and G. Squires, Astrophys. J. **404**, 441 (1993).
[28] P. Schneider, Mon. Not. R. Astron. Soc. **283**, 837 (1996).
[29] D. M. Wittman, J. A. Tyson, D. Kirkman, I. Dell'Antonio, and G. Bernstein, Nature (London) **405**, 143 (2000).
[30] H. Hoekstra, H. K. Yee, and M. D. Gladders, Astrophys. J. **606**, 67 (2004).
[31] N. Okabe, T. Futamase, M. Kajisawa, and R. Kuroshima, Astrophys. J. **784**, 90 (2014).
[32] C. R. Keeton, Astrophys. J. **561**, 46 (2001).
[33] T. Treu, Annu. Rev. Astron. Astrophys. **48**, 87 (2010).
[34] E. Jullo, P. Natarajan, J.-P. Kneib, A. DAloisio, M. Limousin, J. Richard, and C. Schimd, Science **329**, 924 (2010).
[35] A. Klypin, A. V. Kravtsov, O. Valenzuela, and F. Prada, Astrophys. J. **522**, 82 (1999).
[36] B. Willman, F. Governato, J. J. Dalcanton, D. Reed, and T. Quinn, Mon. Not. R. Astron. Soc. **353**, 639 (2004).
[37] E. J. Tollerud, J. S. Bullock, L. E. Strigari, and B. Willman, Astrophys. J. **688**, 277 (2008).
[38] M. J. Rees and J. Ostriker, Mon. Not. R. Astron. Soc. **179**, 541 (1977).
[39] A. Kravtsov, Adv. Astron. **2010**, 281913 (2010).
[40] V. Bromm, Rep. Prog. Phys. **76**, 112901 (2013).
[41] S. Mao and P. Schneider, Mon. Not. R. Astron. Soc. **295**, 587 (1998).
[42] R. B. Metcalf and P. Madau, Astrophys. J. **563**, 9 (2001).
[43] M. Chiba, Astrophys. J. **565**, 17 (2002).
[44] N. Dalal and C. Kochanek, Astrophys. J. **572**, 25 (2002).
[45] R. B. Metcalf and H. Zhao, Astrophys. J. Lett. **567**, L5 (2002).
[46] L. Koopmans, M. Garrett, R. Blandford, C. Lawrence, A. Patnaik, and R. Porcas, Mon. Not. R. Astron. Soc. **334**, 39 (2002).
[47] C. Kochanek and N. Dalal, Astrophys. J. **610**, 69 (2004).
[48] K. T. Inoue and M. Chiba, Astrophys. J. **633**, 23 (2005).
[49] K. T. Inoue and M. Chiba, Astrophys. J. **634**, 77 (2005).

[50] L. Koopmans, Mon. Not. R. Astron. Soc. **363**, 1136 (2005).
[51] J. Chen, E. Rozo, N. Dalal, and J. E. Taylor, Astrophys. J. **659**, 52 (2007).
[52] L. L. Williams, P. Foley, D. Farnsworth, and J. Belter, Astrophys. J. **685**, 725 (2008).
[53] A. More, J. McKean, S. More, R. Porcas, L. Koopmans, and M. Garrett, Mon. Not. R. Astron. Soc. **394**, 174 (2009).
[54] C. R. Keeton and L. A. Moustakas, Astrophys. J. **699**, 1720 (2009).
[55] S. Vegetti and L. V. Koopmans, Mon. Not. R. Astron. Soc. **392**, 945 (2009).
[56] S. Vegetti and L. V. Koopmans, Mon. Not. R. Astron. Soc. **400**, 1583 (2009).
[57] A. B. Congdon, C. R. Keeton, and C. E. Nordgren, Astrophys. J. **709**, 552 (2010).
[58] Y. Hezaveh, N. Dalal, G. Holder, M. Kuhlen, D. Marrone, N. Murray, and J. Vieira, Astrophys. J. **767**, 9 (2013).
[59] S. Vegetti and M. Vogelsberger, Mon. Not. R. Astron. Soc. **442**, 3598 (2014).
[60] Y. Hezaveh, N. Dalal, G. Holder, T. Kisner, M. Kuhlen, and L. P. Levasseur, J. Cosmol. Astropart. Phys. 11 (2016) 048.
[61] Y. D. Hezaveh, N. Dalal, D. P. Marrone, Y.-Y. Mao, W. Morningstar, D. Wen, R. D. Blandford, J. E. Carlstrom, C. D. Fassnacht, G. P. Holder *et al.*, Astrophys. J. **823**, 37 (2016).
[62] R. Feldmann and D. Spolyar, Mon. Not. R. Astron. Soc. **446**, 1000 (2015).
[63] M. Buschmann, J. Kopp, B. R. Safdi, and C.-L. Wu, arXiv:1711.03554.
[64] L. Dai, S.-S. Li, B. Zackay, S. Mao, and Y. Lu, Phys. Rev. D **98**, 104029 (2018).
[65] L. Dai and J. Miralda-Escudé, Astron. J. **159**, 49 (2020).
[66] R. Ibata, G. Lewis, M. Irwin, and T. Quinn, Mon. Not. R. Astron. Soc. **332**, 915 (2002).
[67] K. V. Johnston, D. N. Spergel, and C. Haydn, Astrophys. J. **570**, 656 (2002).
[68] J. M. Siegal-Gaskins and M. Valluri, Astrophys. J. **681**, 40 (2008).
[69] J. Bovy, Phys. Rev. Lett. **116**, 121301 (2016).
[70] R. G. Carlberg, Astrophys. J. **820**, 45 (2016).
[71] D. Erkal, V. Belokurov, J. Bovy, and J. L. Sanders, Mon. Not. R. Astron. Soc. **463**, 102 (2016).
[72] A. Bonaca and D. W. Hogg, Astrophys. J. **867**, 101 (2018).
[73] A. Bonaca, D. W. Hogg, A. M. Price-Whelan, and C. Conroy, Astrophys. J. **880**, 38 (2019).
[74] N. Banik, J. Bovy, G. Bertone, D. Erkal, and T. J. L. de Boer, arXiv:1911.02662.
[75] B. Paczynski, Astrophys. J. **304**, 1 (1986).
[76] C. Alcock, R. Allsman, D. R. Alves, T. Axelrod, A. C. Becker, D. Bennett, K. H. Cook, N. Dalal, A. J. Drake, K. Freeman *et al.*, Astrophys. J. **542**, 281 (2000).
[77] P. Tisserand, L. Le Guillou, C. Afonso, J. Albert, J. Andersen, R. Ansari, É. Aubourg, P. Bareyre, J. Beaulieu, X. Charlot *et al.*, Astron. Astrophys. **469**, 387 (2007).
[78] K. Griest, A. M. Cieplak, and M. J. Lehner, Astrophys. J. **786**, 158 (2014).
[79] H. Niikura, M. Takada, N. Yasuda, R. H. Lupton, T. Sumi, S. More, T. Kurita, S. Sugiyama, A. More, M. Oguri *et al.*, Nat. Astron. **3**, 524 (2019).
[80] M. Zumalacarregui and U. Seljak, Phys. Rev. Lett. **121**, 141101 (2018).
[81] E. R. Siegel, M. Hertzberg, and J. Fry, Mon. Not. R. Astron. Soc. **382**, 879 (2007).
[82] N. Seto and A. Cooray, Astrophys. J. Lett. **659**, L33 (2007).
[83] S. Baghram, N. Afshordi, and K. M. Zurek, Phys. Rev. D **84**, 043511 (2011).
[84] K. Kashiyama and N. Seto, Mon. Not. R. Astron. Soc. **426**, 1369 (2012).
[85] H. A. Clark, G. F. Lewis, and P. Scott, Mon. Not. R. Astron. Soc. **456**, 1394 (2016).
[86] K. Schutz and A. Liu, Phys. Rev. D **95**, 023002 (2017).
[87] J. A. Dror, H. Ramani, T. Trickle, and K. M. Zurek, Phys. Rev. D **100**, 023003 (2019).
[88] K. Van Tilburg, A.-M. Taki, and N. Weiner, J. Cosmol. Astropart. Phys. 07 (2018) 041.
[89] P. Ade, N. Aghanim, M. Arnaud, F. Arroja, M. Ashdown, J. Aumont, C. Baccigalupi, M. Ballardini, A. Banday, R. Barreiro *et al.*, Astron. Astrophys. **594**, A20 (2016).
[90] Y. Akrami, F. Arroja, M. Ashdown, J. Aumont, C. Baccigalupi, M. Ballardini, A. Banday, R. Barreiro, N. Bartolo, S. Basak *et al.*, Astrophys. Space Sci. **364**, 69 (2019).
[91] S. Bird, H. V. Peiris, M. Viel, and L. Verde, Mon. Not. R. Astron. Soc. **413**, 1717 (2011).
[92] P. Colin, V. Avila-Reese, and O. Valenzuela, Astrophys. J. **542**, 622 (2000).
[93] P. Bode, J. P. Ostriker, and N. Turok, Astrophys. J. **556**, 93 (2001).
[94] M. Viel, J. Lesgourgues, M. G. Haehnelt, S. Matarrese, and A. Riotto, Phys. Rev. D **71**, 063534 (2005).
[95] W. Hu, R. Barkana, and A. Gruzinov, Phys. Rev. Lett. **85**, 1158 (2000).
[96] B. Li, T. Rindler-Daller, and P. R. Shapiro, Phys. Rev. D **89**, 083536 (2014).
[97] L. Hui, J. P. Ostriker, S. Tremaine, and E. Witten, Phys. Rev. D **95**, 043541 (2017).
[98] B. J. Carr, Astrophys. J. **201**, 1 (1975).
[99] J. C. Niemeyer and K. Jedamzik, Phys. Rev. D **59**, 124013 (1999).
[100] M. S. Delos, A. L. Erickcek, A. P. Bailey, and M. A. Alvarez, Phys. Rev. D **97**, 041303 (2018).
[101] M. S. Delos, A. L. Erickcek, A. P. Bailey, and M. A. Alvarez, Phys. Rev. D **98**, 063527 (2018).
[102] V. Berezinsky, V. Dokuchaev, and Y. Eroshenko, J. Cosmol. Astropart. Phys. 11 (2013) 059.
[103] K. M. Zurek, C. J. Hogan, and T. R. Quinn, Phys. Rev. D **75**, 043511 (2007).
[104] M. Buschmann, J. W. Foster, and B. R. Safdi, arXiv: 1906.00967.
[105] L. Dai and J. Miralda-Escud, Astron. J. **159**, 49 (2020).
[106] A. Arvanitaki, S. Dimopoulos, M. Galanis, L. Lehner, J. O. Thompson, and K. Van Tilburg, Phys. Rev. D **101**, 083014 (2020).
[107] P. Agrawal and L. Randall, J. Cosmol. Astropart. Phys. 12 (2017) 019.

[108] J. H. Chang, D. Egana-Ugrinovic, R. Essig, and C. Kouvaris, J. Cosmol. Astropart. Phys. 03 (2019) 036.
[109] R. Essig, S. D. McDermott, H.-B. Yu, and Y.-M. Zhong, Phys. Rev. Lett. **123**, 121102 (2019).
[110] See Supplemental Material at http://link.aps.org/supplemental/10.1103/PhysRevLett.125.111101, which includes a complete derivation of the test-statistic, a detailed description of the data processing, analysis, and signal simulations.
[111] P. J. McMillan, Mon. Not. R. Astron. Soc. **414**, 2446 (2011).
[112] T. Prusti, J. De Bruijne, A. G. Brown, A. Vallenari, C. Babusiaux, C. Bailer-Jones, U. Bastian, M. Biermann, D. W. Evans, L. Eyer *et al.*, Astron. Astrophys. **595**, A1 (2016).
[113] A. Brown, A. Vallenari, T. Prusti, J. De Bruijne, C. Babusiaux, C. Bailer-Jones, M. Biermann, D. W. Evans, L. Eyer, F. Jansen *et al.*, Astron. Astrophys. **616**, A1 (2018).
[114] S. Chen, H. Richer, I. Caiazzo, and J. Heyl, Astrophys. J. **867**, 132 (2018).
[115] L. Lindegren, Gaia Technical Note: GAIA-C3-TN-LU-LL-124-01, 2018.
[116] X. Luri, A. G. A. Brown, L. M. Sarro, F. Arenou, C. A. L. Bailer-Jones, A. Castro-Ginard, J. de Bruijne, T. Prusti, C. Babusiaux, and H. E. Delgado, Astron. Astrophys. **616**, A9 (2018).
[117] F. Arenou, X. Luri, C. Babusiaux, C. Fabricius, A. Helmi, T. Muraveva, A. Robin, F. Spoto, A. Vallenari, T. Antoja *et al.*, Astron. Astrophys. **616**, A17 (2018).
[118] L. Lindegren, J. Hernández, A. Bombrun, S. Klioner, U. Bastian, M. Ramos-Lerate, A. De Torres, H. Steidelmüller, C. Stephenson, D. Hobbs *et al.*, Astron. Astrophys. **616**, A2 (2018).
[119] G. Gyuk, N. Dalal, and K. Griest, Astrophys. J. **535**, 90 (2000).
[120] C. J. Evans and I. D. Howarth, Mon. Not. R. Astron. Soc. **386**, 826 (2008).
[121] E. Nadler *et al.* (DES Collaboration), Astrophys. J. **893**, 48 (2020).
[122] E. Patel, N. Kallivayalil, N. Garavito-Camargo, G. Besla, D. R. Weisz, R. P. van der Marel, M. Boylan-Kolchin, M. S. Pawlowski, and F. A. Gómez, Astrophys. J. **893**, 121 (2020).
[123] J. I. Read, M. Wilkinson, N. Evans, G. Gilmore, and J. T. Kleyna, Mon. Not. R. Astron. Soc. **366**, 429 (2006).
[124] J. Binney and S. Tremaine, *Galactic Dynamics* (Princeton University Press, Princeton, NJ, 2011).